STRESS CORROSION CRACKING SUSCEPTIBILITY OF IRRADIATED TYPE 304 STAINLESS STEELS*

by

H. M. Chung, W. E. Ruther, J. E. Sanecki, and T. F. Kassner

Materials and Components Technology Division
Argonne National Laboratory
Argonne, IL 60439

ANL/MCT/CP--74743

DE93 003005

DISCLAIMER

August 1992

Received by OSTI

NOV 1 6 1992

Presented at the Sixteenth International Symposium on Effects of Radiation on Materials, June 21-25, 1992, Denver, Colorado.

*Work supported by the U.S. Nuclear Regulatory Commission, Office of Nuclear Regulatory Research.

STRESS CORROSION CRACKING SUSCEPTIBILITY OF IRRADIATED TYPE 304 STAINLESS STEELS*

by

H. M. Chung, W. E. Ruther, J. E. Sanecki, and T. F. Kassner
Materials and Components Technology Division
Argonne National Laboratory
Argonne, IL 60439

ABSTRACT: Slow-strain-rate tensile tests and microstructural analysis by Auger electron spectroscopy were conducted on specimens of high- and commercial-purity (HP and CP) heats of Type 304 stainless steel obtained from neutron absorber tubes and a control blade sheath after irradiation up to 2.5×10^{21} n·cm^{-2} (E>1 MeV) in boiling water reactors (BWRs). The susceptibility of the HP absorber tubes to intergranular stress corrosion cracking (IGSCC) was higher than that of the CP absorber tubes or the CP control blade sheath. IGSCC susceptibilities of the BWR components could not be correlated to segregation impurities on grain boundaries. However, for comparable fluence levels, the susceptibilities could be correlated to concentrations of Cr on grain-boundaries.

KEY WORDS: boiling water reactor, austentic stainless steels, irradiation-assisted stress corrosion cracking, slow-strain-rate tensile tests, Auger electron spectroscopy, intergranular failure, grain-boundary segregation and depletion

In recent years, failures of nonsensitized austenitic stainless steel (SS) core internal components in both boiling- and pressurized-water reactors (BWRs and PWRs) have increased after accumulation of relatively high fluence (>5 x 10^{20} n·cm^{-2}, E >1 MeV). Although most failed components can be replaced, some safety-significant structural components, such as the BWR top guide, shroud, and core plate, would be very difficult or impractical to replace. Therefore, the structural integrity of these components after accumulation of high fluence has been a subject of concern, and extensive research has been conducted to provide an understanding of this type of degradation, which is commonly known as irradiation-assisted stress corrosion cracking (IASCC).[1-21] Component fabrication and reactor operational parameters, such as neutron flux, fluence, temperature, water chemistry, residual stress, and mechanical loads, have been reported to influence susceptibility to IASCC. However, results from research at several laboratories on materials irradiated under a wide variety of simulated conditions are often inconsistent and conflicting as to the influence of these parameters.[3,10]

IASCC failures have been attributed to radiation-induced segregation (RIS) or depletion of impurity and alloying elements at grain boundaries. Grain boundary RIS of P,[4,7,8,16] Si,[4,7-9,16] and an unidentified element giving rise to 59-eV in Auger electron spectroscopy (AES),[16] and Cr depletion[7-9,16,17] have been reported by several investigators, but RIS of S,[7,8,16] C, and N has not been confirmed. However, the relative importance of the roles of RIS of impurities and Cr depletion in IASCC is far from clear and often conflicting.[7,8,16-21]

In-reactor[2] and laboratory experience[8] showed a high-purity (HP) heat of Type 348 SS performed better than a commercial-purity (CP) heat (containing relatively high C, Si, P, and N); the better performance was thought to indicate that RIS of Si is the predominant process, because RIS of other impurities and Cr depletion in the HP and CP Type 348 SS were either similar or could not be detected from analysis by field-emission-gun scanning transmission electron microscopy (FEG-STEM).[8] These experiences with Type 348 SS have led to the observation that in-reactor IASCC performance can be duplicated by constant-extension-rate tests (CERT) in the laboratory.[8] It has also been reported that, after irradiation in a test reactor, Type 316L SS exhibited somewhat better resistance to stress corrosion cracking (SCC) than Type 316NG SS,[5] indicating a possible benefit of low N. On the basis of the experiences with Type 348 and 316 SS, HP Type 304 SS has been suggested as a better alternative to CP Type 304 SS. However, the superior performance of HP Type 304 SS has not been established, although there is an indication of better resistance of HP Type 304 SS neutron absorber rods relative to CP heat in an uncreviced environment in BWR.[14]

In the present study, CERT tests were conducted on specimens obtained from BWR neutron absorber tubes and a control blade sheath fabricated from two heats of HP- and two heats of CP-grade Type 304 SS. Results from the CERT tests were correlated with results of microstructural analysis by AES to identify the primary process that controls susceptibility to IGSCC and in-reactor performance of Type 304 SS components.

Experimental Procedures

Specimen preparation, procedures for slow-strain-rate tensile (SSRT) tests, and a description of the hot-cell SSRT apparatus were given in previous reports.[11-13,16] Cylindrical specimens, 89 mm long, were sectioned from top-, middle-, and bottom-axial positions of BWR neutron absorber rods, and boron carbide was removed with diamond-tip drills. Maximum fluence at the top was determined from known in-reactor flux data. Lower fluences at the other two axial locations were determined from results of ^{60}Co gamma scans of the entire length of the rods. Tensile specimens, 57.2 mm long, 12.7 mm wide, and 1.22 mm thick, were fabricated from a BWR control blade sheath. The length of the 3.2-mm-wide gage section of the sheath specimens was ≈19.1 mm. The fast neutron fluence and chemical composition of the HP and CP heats of Type 304 SS are given in Table 1. Documentation of the chemical composition of the CP-grade neutron absorber and control blade sheath were not available from either the utility or the reactor-fuel supplier. Compositions of the three HP heats are similar except for N content.

SSRT tests were conducted in air and in simulated BWR water at 289°C at a strain rate of 1.65×10^{-7} s^{-1}. The dissolved O concentration and conductivity of the simulated BWR water were ≈300 ppb and 0.12 $\mu S \cdot cm^{-1}$, respectively (Table 2). Analysis of fracture surface of SSRT specimens was conducted by scanning electron microscopy (SEM) to determine the types of fracture surface morphology, whereas the chemical composition of precipitates was determined by energy dispersive X-ray spectroscopy (EDS). Fractography by SEM was conducted at magnifications of 60 to 800X, and an entire fracture-surface composite was constructed for each specimen to determine the fraction of intergranular, transgranular, and ductile failure.

Grain-boundary microchemistry was analyzed with a JEOL Company JAMP-10 Model scanning Auger microscope (SAM). Specimens charged with H were fractured at room

Table 1. Chemical Composition and Fluence of High- and Commercial-Purity Type 304 Stainless Steel BWR Components

Material and Heat	Composition (wt.%)									Compon. Code	Service Reactor	Fluence, 10^{21} n cm^{-2}
	Cr	Ni	Mn	C	N	B	Si	P	S			
HP304 -A	18.50	9.45	1.53	0.018	0.100	<0.001	<0.03	0.005	0.003	V-AT[a]	BWR-B	0.2-1.4
HP304-B	18.30	9.75	1.32	0.015	0.080	<0.001	0.05	0.005	0.005	V-AT[a]	BWR-B	0.2-1.4
HP304-CD	18.58	9.44	1.22	0.017	0.037	0.001	0.02	0.002	0.003	V-AT[a]	BWR-B	0.2-1.4
										QC-AT[b]	BWR-QC	2.0
CP304 -A	16.80	8.77	1.65	0.08[c]	0.052	-	1.55	0.045[c]	0.030[c]	BL-AT[d]	BWR-Y	0.2-2.0
CP304 -B	18-20	8-10.5	2.00[c]	0.08[c]	-	-	1.00[c]	0.045[c]	0.030[c]	LC-S[e]	BWR-LC	0.5-2.6

[a]High-purity neutron absorber tubes, OD = 4.78 mm, wall thickness = 0.63 mm, composition measured before service.
[b]High-purity neutron absorber tubes, OD = 4.78 mm, wall thickness = 0.63 mm, composition measured before service.
[c]Represents maximum value in the specification; actual value not measured.
[d]Commercial-purity neutron absorber tubes, OD = 4.78 mm, wall thickness = 0.79 mm, composition measured after service.
[e]Commercial-purity control blade sheath, thickness 1.22 mm, actual composition not measured.

Table 2. SSRT[a] Test Results on Irradiated Commercial- and High-Purity Type 304 SS BWR Neutron Absorber Tubes and Control Blade Sheath in Air and High-Purity Water Containing 280 ppb Dissolved Oxygen at 289°C

Specimen Ident. No.	Hot-cell Ident. No.	Source Heat Ident. No.	Fast-Neutron Fluence, n·cm^{-2}	SSRT No.	Water Chemistry[b]		SSRT Parameters				
					Oxygen Conc., ppb	Cond. at 25°C, μS·cm^{-1}	Failure Time, h	Max. Stress, MPa	Total Elong., %	TGSCC, %	IGSCC, %
BL-BWR-2H	389E3A	CP304-A	2.0×10^{21}	IR-9	c	c	228	631	13.5	0	0
BL-BWR-2H	389E3D	CP304-A	2.0×10^{21}	IR-12	300	0.13	21	415	1.2	8	28
BL-BWR-2M	389E2D	CP304-A	0.6×10^{21}	IR-3	c	c	580	465	34.8	0	0
BL-BWR-2M	389E2A	CP304-A	0.6×10^{21}	IR-8	290	0.15	140	359	8.3	55	0
BL-BWR-2L	389E1A	CP304-A	0.2×10^{21}	IR-2	c	c	260	390	15.6	0	0
BL-BWR-2L	389E1D	CP304-A	0.2×10^{21}	IR-1	280	0.13	107	337	6.7	43	0
VH-A7A-L2	406A1F	HP304-A	1.4×10^{21}	IR-5	c	c	93	786	5.6	0	0
VH-A7A-L1	406A1E	HP304-A	1.4×10^{21}	IR-4	280	0.10	11	417	0.6	2	58
VM-D5B-L2	406C3	HP304-CD	0.7×10^{21}	IR-6	c	c	405	684	24.2	0	0
VM-D5B-L1	406C2	HP304-CD	0.7×10^{21}	IR-7	280	0.12	31	552	1.8	8	34
VL-A4C-L2	406B3	HP304-A	0.2×10^{21}	IR-10	c	c	231	607	13.7	0	0
VL-A4C-L1	406B2	HP304-A	0.2×10^{21}	IR-11	330	0.14	77	520	4.6	47	14
C71U	LSC-1	CP304-B	2.45×10^{21}	IR-15	c	c	123	830	7.3	-	-
C71X	LSC-2	CP304-B	2.26×10^{21}	IR-16	310	0.12	74	841	4.2	2	3
C72T	LCS-4	CP304-B	2.54×10^{21}	IR-13	c	c	121	876	7.2	-	-
C72S	LCS-3	CP304-B	2.64×10^{21}	IR-14	320	0.11	84	843	5.0	2	4
C7T1T	LSC-7	CP304-B	1.59×10^{21}	IR-19	c	c	203	792	12.0	-	-
C7T1J	LCS-8	CP304-B	1.53×10^{21}	IR-20	360	0.11	101	872	6.1	3	6
C7B1W	LCS-5	CP304-B	0.23×10^{21}	IR-17	c	c	574	577	34.1	-	-
C7B1X	LSC-6	CP304-B	0.20×10^{21}	IR-18	310	0.11	457	572	27.1	8	0

[a]Strain rate of 1.65×10^{-7} s^{-1}.
[b]pH at 25°C 6.22-6.33.
[c]Test in air at 289°C and strain rate of 1.65×10^{-7} s^{-1}.

temperature in the ultrahigh vacuum (≈7 to 20 x 10^{-7} Pa) of the SAM. Depth profiles were obtained as a function of sputter distance beneath a selected region of intergranular fracture. The sputter (by Ar ion) removal rate was ≈0.2-0.4 nm·s^{-1}. Typically, a selected surface was sputtered for 2-4 s and then an Auger spectrum was obtained for 100-110 s on a freshly sputtered surface 1-2 s after sputtering. The entire procedure was automated and computer-controlled.

Results

SSRT Tests

Test conditions, SSRT test data, and SEM analyses are summarized in Table 2. Stress-vs.-elongation curves of the CP absorber, HP absorber, and CP sheath specimens are shown in Figs 1-3, respectively. The figures portray SSRT test data for high-, medium-, and low-fluence specimens strained to failure in simulated BWR water and air. As fluence increased, the ratio of elongation in water to that in air became smaller, indicating a greater degree of SCC.

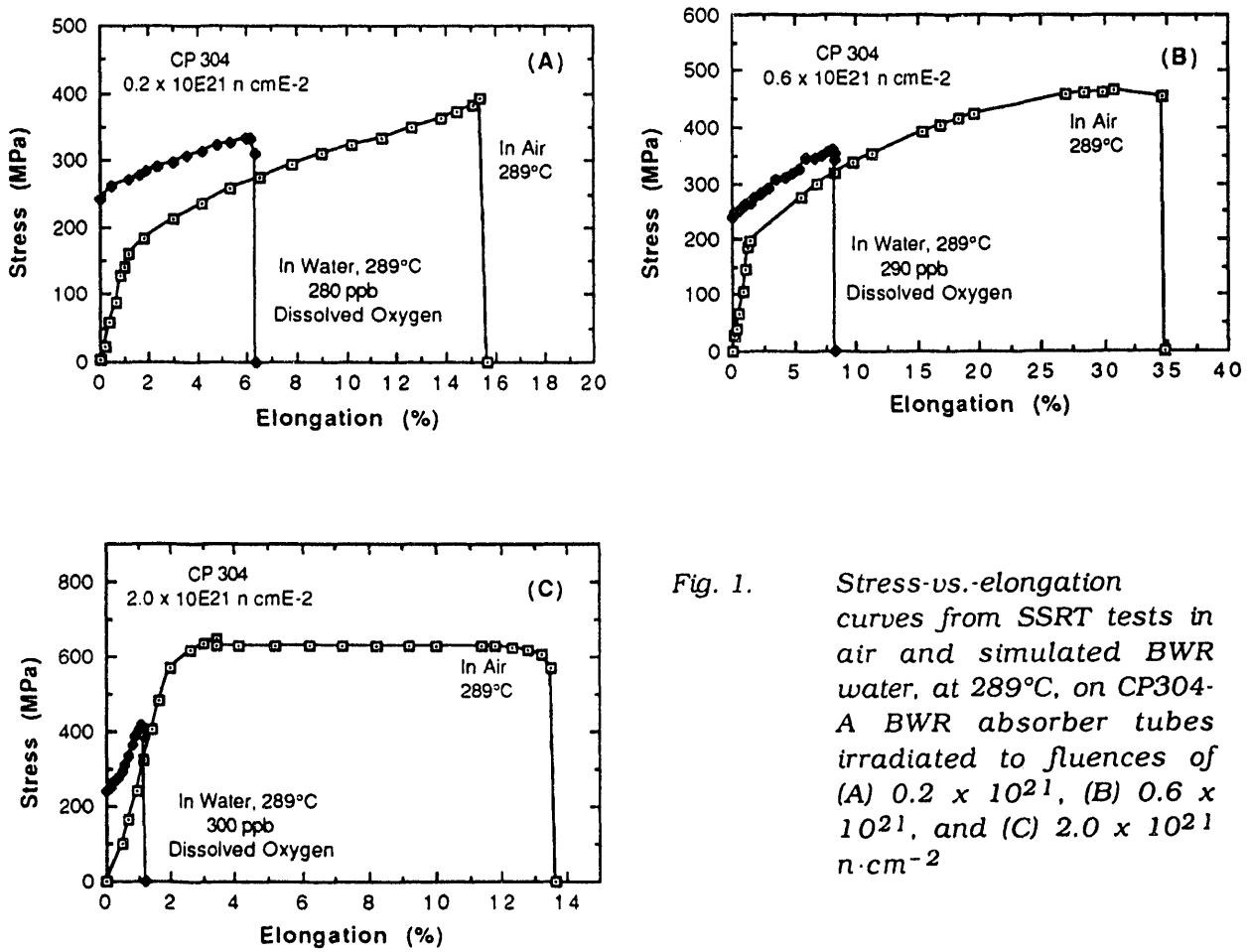

Fig. 1. Stress-vs.-elongation curves from SSRT tests in air and simulated BWR water, at 289°C, on CP304-A BWR absorber tubes irradiated to fluences of (A) 0.2 x 10^{21}, (B) 0.6 x 10^{21}, and (C) 2.0 x 10^{21} n·cm^{-2}

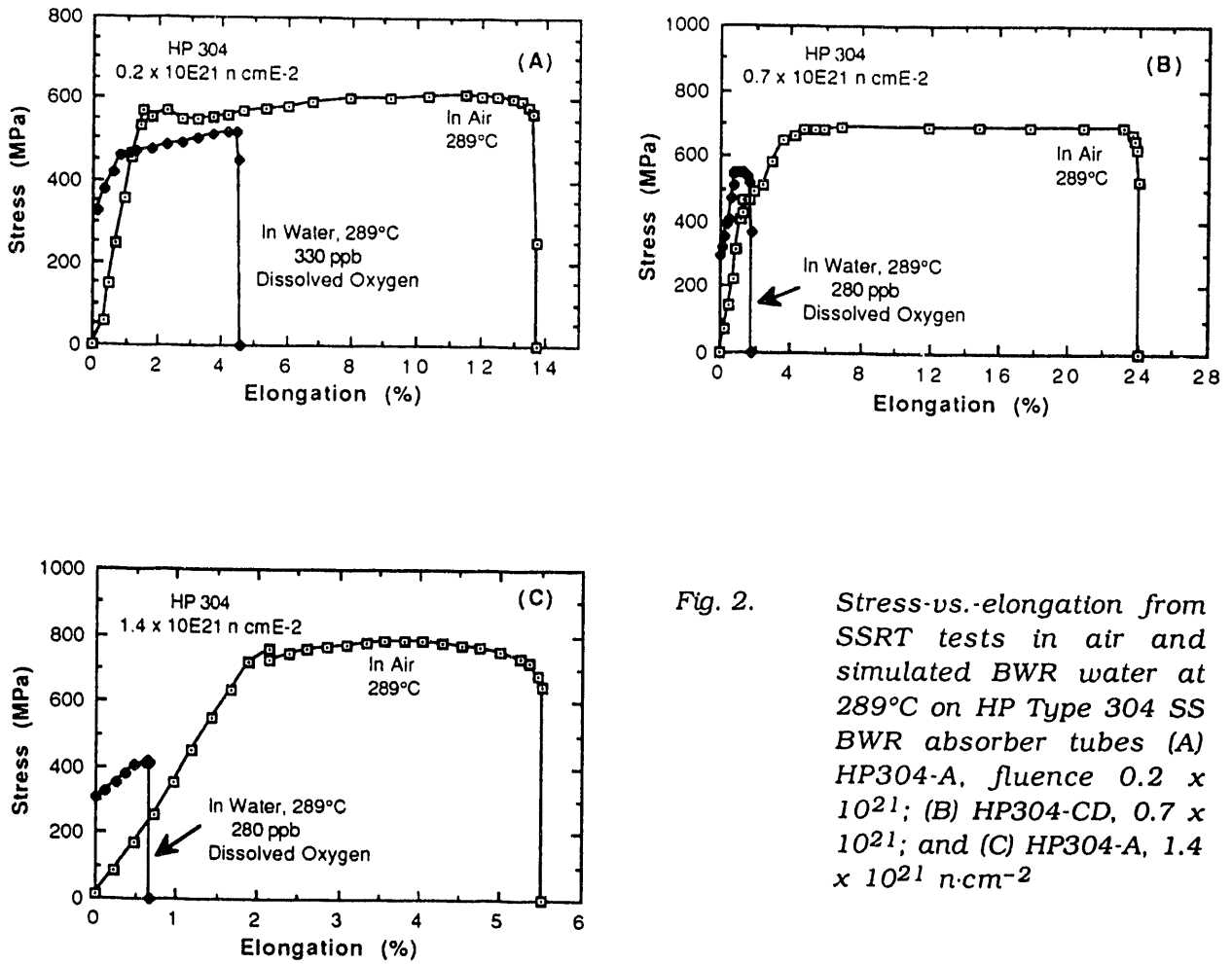

Fig. 2. *Stress-vs.-elongation from SSRT tests in air and simulated BWR water at 289°C on HP Type 304 SS BWR absorber tubes (A) HP304-A, fluence 0.2 x 10^{21}; (B) HP304-CD, 0.7 x 10^{21}; and (C) HP304-A, 1.4 x 10^{21} n·cm^{-2}*

Both the yield and ultimate tensile strengths of the HP absorber tubes and CP sheath at the high fluence were significantly higher than those of the CP neutron absorber or the specimens irradiated in the Advanced Test Reactor (ATR).[5] Tensile strength of the CP sheath specimens was similar to that of the HP neutron absorber tubes for comparable fluence. HP Heat-A and -CD absorber tubes, irradiated in BWR-B and -QC, respectively, and CP Heat-B sheath, irradiated in BWR-LC, contained high density of small (≈20-40 μm) precipitates. Results of AES revealed that the precipitates are rich in Cu, N, C, and S. The high strength of the HP absorber tubes and the CP sheath may be associated with these precipitates, which apparently formed during irradiation. Whereas the strength of the ATR-irradiated materials tends to reach saturation at a fluence ≥1.5 x 10^{21} n cm^{-2}, the strength of BWR components seemed to reach saturation at a significantly higher fluence. Ductility appears to reach an asymptotic minimum value of ≈5% at fluence levels >1.5 x 10^{21} n·cm^{-2}. Total elongation of the BWR-irradiated material is, however, considerably smaller than that of the ATR-irradiated materials at the high fluence level, i.e. 5-10 vs. 8-22 %.

The percent intergranular and transgranular SCC (IGSCC and TGSCC) was measured from the SEM fracture surface map; the results are given in Table 2. The fraction of IGSCC

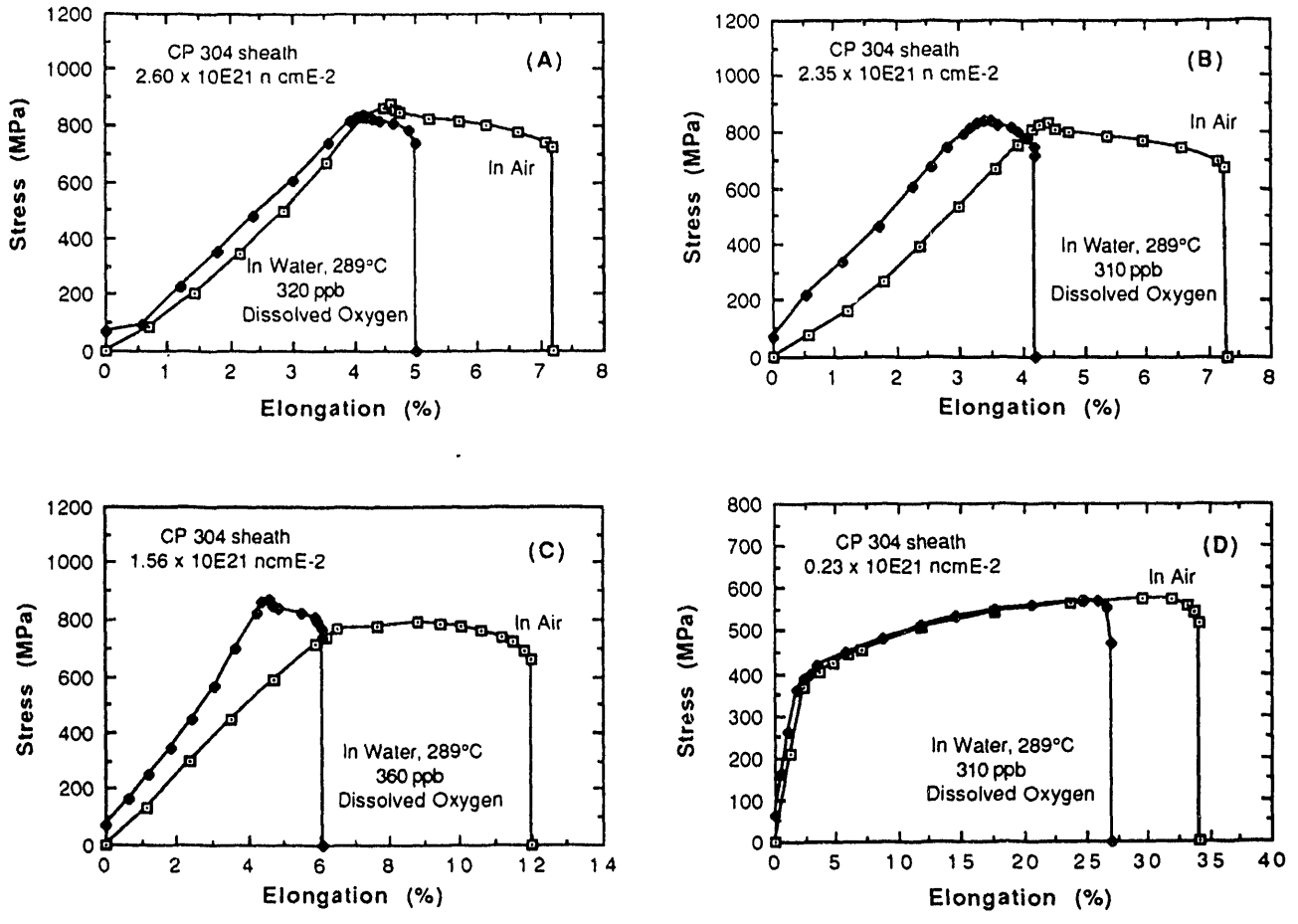

Fig. 3. Stress-vs.-elongation curves from SSRT tests in air and simulated BWR water at 289°C on CP304-B control blade sheath irradiated to fluences of (A) 2.60 x 10^{21}, (B) 2.35 x 10^{21}, (C) 1.59 x 10^{21}, and (D) 0.23 x 10^{21} n·cm^{-2}

in the CP304-B sheath specimens irradiated to fluence of ≈2.5 x 10^{21} n cm^{-2} was only 3-4 %. This was significantly lower than the IGSCC fraction in the CP304-A or HP304-A and HP304-CD absorber tubes. In general, the percent IGSCC determined from SEM fractography could be correlated well with either total elongation or the ratio of elongation in water and air. However, susceptibility to IGSCC could not be correlated well with increase in yield strength (i.e., as-irradiated yield strength minus as-fabricated yield strength).

The percent IGSCC vs. neutron fluence for the CP absorber tubes and control blade sheath was comparable to similar data obtained on CP heats of Types 304 and 316 SS.[1,5,15] The materials in the study by Jacobs et al.[5] were irradiated at 300°C in the ATR, whereas the specimens tested by Kodama et al.[15] were from BWR-irradiated dry tubes. The SSRT

tests in all of the studies were conducted at 289°C in simulated BWR water containing several different concentrations of dissolved O , i.e., 0.3, 8, or 32 ppm. Despite the wide range of strain rates and dissolved-O concentrations in the various tests, the dependence of percent IGSCC on neutron fluence was reasonably consistent.

A comparison of the percent IGSCC vs. fast-neutron fluence (E >1 MeV) for the present CP and HP neutron absorber tubes and CP control blade sheath is shown in Fig. 4, along with similar results from SSRT tests on CP-grade BWR dry tubes reported by Kodama et al.[15] All of these data were obtained at a strain rate of ≈2 x 10^{-7} s^{-1} in water containing ≈0.2-0.3 ppm dissolved oxygen. The figure indicates that the susceptibility of the CP304-B control blade sheath to IGSCC is significantly lower than that of the CP304-A neutron absorber tube or the dry tube of Kodama et al.[15] for comparable fluence levels. However, the susceptibilities of the HP304-A and -CD absorber tubes are similar despite the significant difference in N content (i.e. 0.10 vs. 0.037 wt%, respectively). The susceptibilities of the HP materials are significantly greater than those of the CP materials. This appears to be consistent with results obtained from proton-[18] and ion-irradiated[19] HP and CP materials of Type 304 SS.

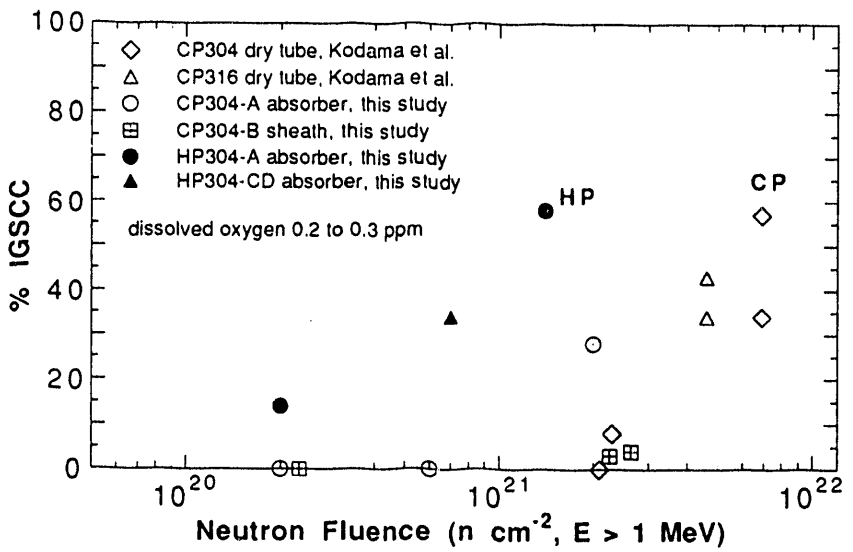

Fig. 4. Percent IGSCC vs. fluence (E >1 MeV) for HP Type 304 SS and CP Type 304 and 316 SS BWR components from SSRT tests at 289°C in simulated BWR water containing ≈300 ppb dissolved O. showing that the HP material is more susceptible to IGSCC than the CP material.

AES Analysis

For comparable fluence and hydrogen charging time, it was surprisingly easier to produce intergranular fracture in AES specimens from the HP304-CD absorber tubes

irradiated in BWR-QC than in specimens from the HP304-A absorber tubes irradiated in BWR-B. Compared with other heats listed in Table 1 and irradiated to a similar fluence of $\approx 2 \times 10^{21}$ n cm^{-2}, it was conspicuously difficult to produce intergranular fracture in vacuo in the absorber tubes fabricated from the latter HP heat. The reason of this trend, which is the opposite of the relative IGSCC susceptibility during SSRT tests in water (Fig. 4), is not known.

Auger signals from several spots on ductile and intergranular fracture regions were analyzed, and peak-to-peak amplitudes of the primary peaks of Ni, Si, P, C, N, S, and the unidentified $X_{59\text{-}eV}$ peak[16] were measured and normalized with respect to the amplitude of the primary peak of Fe. The results obtained for CP304-A, CP304-B, HP304-A, and HP304-CD specimens irradiated to $\approx 2 \times 10^{21}$ n cm^{-2} are shown in Figs. 5 to 8, respectively. Significant grain-boundary segregation of Ni, Si, P, and the unidentified $X_{59\text{-}eV}$ element in the CP absorber tube and sheath is evident. In the CP304-B sheath specimen, there was an indication of C segregation (Fig. 6E). No evidence of N or S segregation was observed in either the CP sheath or the CP absorber tube specimen.

In distinct contrast to the CP sheath specimens, segregation of Si or P in the HP304-A specimen irradiated to a fluence of $\approx 1.4 \times 10^{21}$ n cm^{-2} was negligible (Fig 7), although some segregation of the elements was detectable in the HP304-CD specimen irradiated to $\approx 2.0 \times 10^{21}$ n cm^{-2} (Fig. 8). Compared with the HP304-A specimens, segregation of the unidentified $X_{59\text{-}eV}$ element in the HP304-CD specimen was significant, a behavior similar to that of CP304-A and -B specimens. It is not clear if this segregation of the unidentified $X_{59\text{-}eV}$ element is related to the relatively easier production of intergranular fracture in vacuo in the latter three heats than in HP304-A.

In the HP304-CD specimen irradiated to $\approx 2.0 \times 10^{21}$ n cm^{-2}, segregation of N by a factor of ≈ 1.5-1.9 was also detected (Fig. 8F). Despite the higher N content in Heat HP304-A, N segregation was not evident in this heat when irradiated to $\approx 1.4 \times 10^{21}$ n cm^{-2}. Segregation of C and S was not detected in either of the HP heats. The intensity of the S peak was, in general, stronger in a specimen that was fractured after H charging and Cu plating than in a specimen fractured in the absence of the Cu-plating step. Apparently, higher S contamination occurred during Cu plating because an S-containing solution was used in the Cu-plating process.

As pointed out previously, distribution of Cr near a grain boundary could be characterized only by the sputter depth-profile technique.[16] Cr depletion profiles obtained from specimens of the CP304-A and HP304-A are shown in Figs. 9A and 9B, respectively, whereas Fig. 9(C) shows results obtained from CP304-B and HP304-CD irradiated to a fluence of $\approx 2.0 \times 10^{21}$ n cm^{-2}. These figures show that Cr depletion is more pronounced in the HP heats than in the CP heats for comparable fluence level. Based on the Cr depletion profiles in Fig. 9 and bulk Cr compositions, minimum Cr contents on grain boundaries of the CP and HP absorber tubes and control blade sheath were determined; the results are summarized in Table 3.

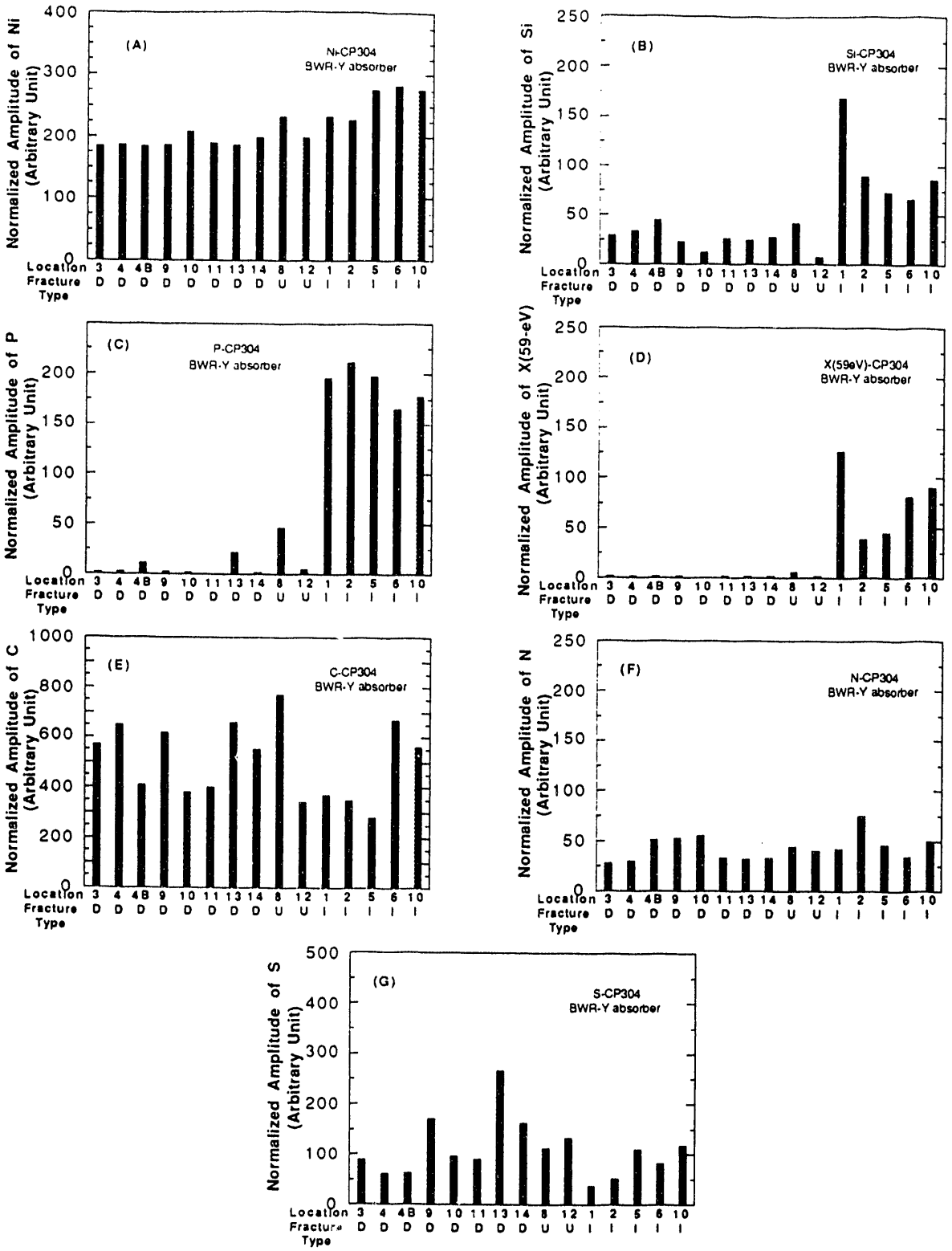

Fig 5. Normalized amplitudes of (a) Ni, (b) Si, (c) P, (d) an unidentified element (denoted $X_{59\text{-}eV}$), (e) C, (f) N, and (g) S that were obtained from ductile- (denoted by letter D) and intergranular- (I) fracture surfaces of CP Heat 304-A absorber tube irradiated to fluence of ≈2.0 x 10^{21} n cm^{-2} (E >1 MeV). Letter U denotes faceted fracture surfaces of uncertain type.

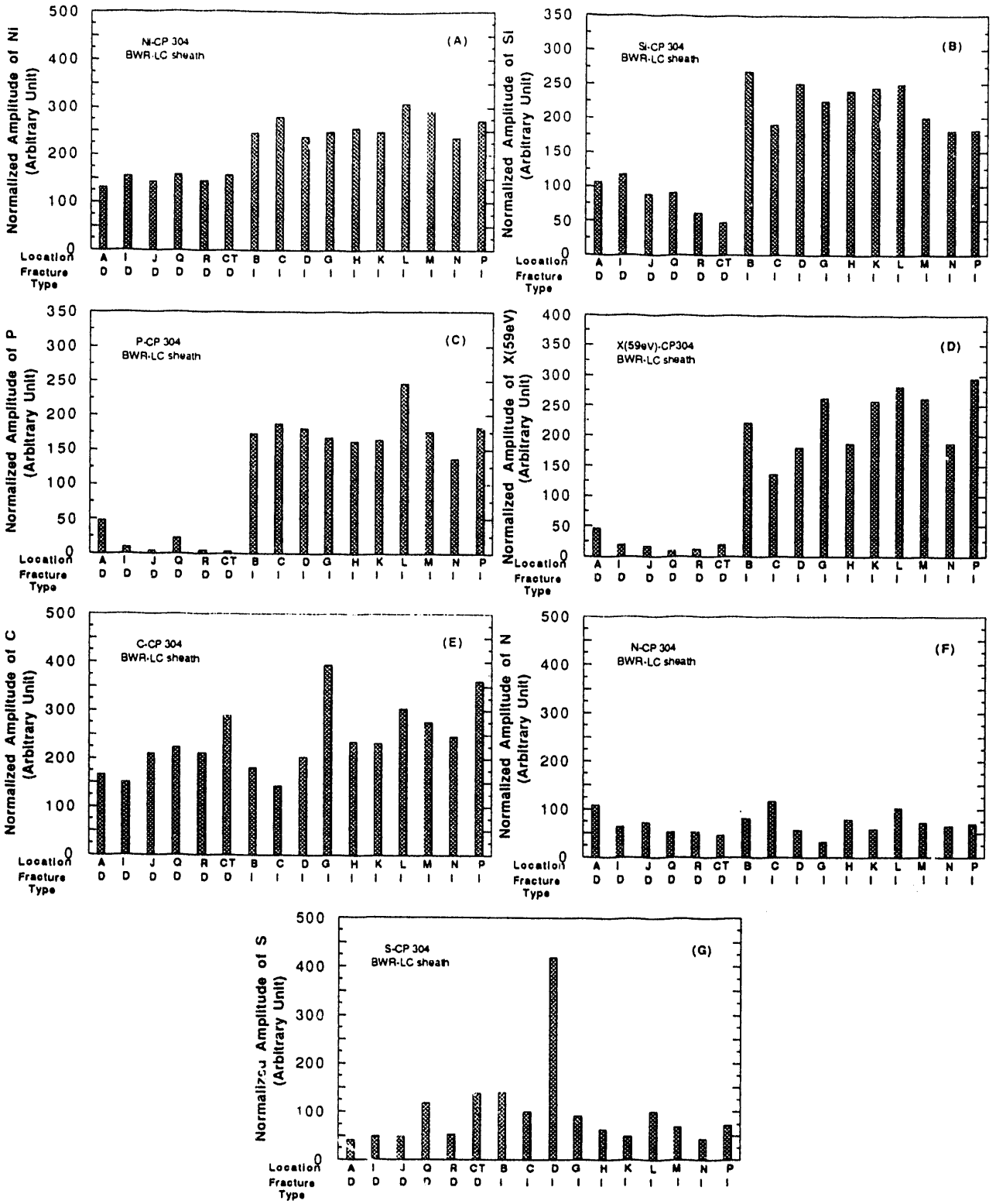

Fig 6. Normalized amplitudes of (a) Ni, (b) Si, (c) P, (d) an unidentified element (denoted $X_{59\text{-}eV}$), (e) C, (f) N, and (g) S that were obtained from ductile- (denoted by letter D) and intergranular- (I) fracture surfaces of CP Heat 304-B absorber tube irradiated to fluence of ≈2.0 x 10^{21} n cm^{-2} (E >1 MeV).

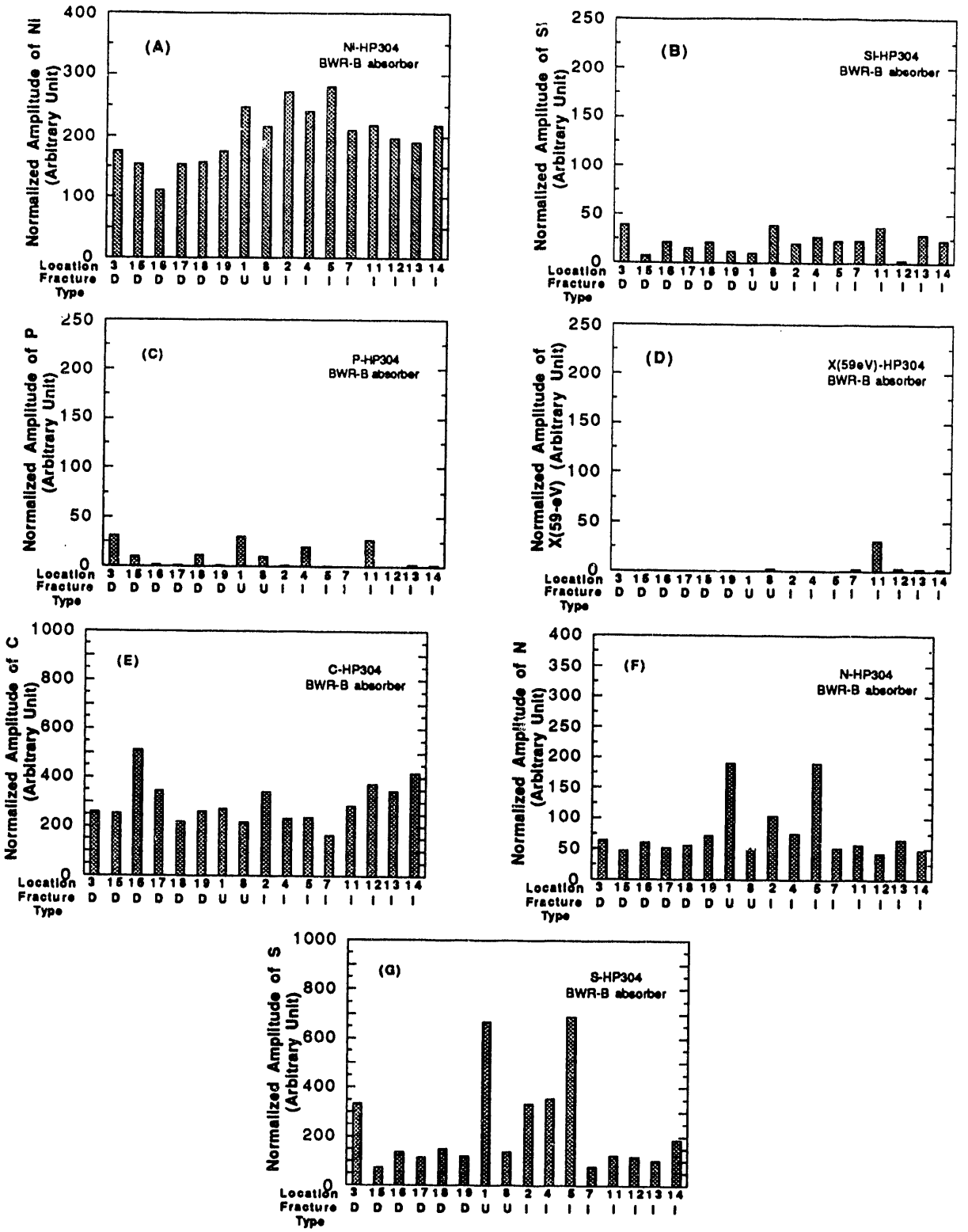

Fig 7. Normalized amplitudes of (a) Ni, (b) Si, (c) P, (d) an unidentified element (denoted $X_{59\text{-}eV}$), (e) C, (f) N, and (g) S that were obtained from ductile- (denoted by letter D) and intergranular- (I) fracture surfaces of HP Heat 304-A absorber tube irradiated to fluence of ≈1.4 x 10^{21} n cm^{-2} (E >1 MeV).

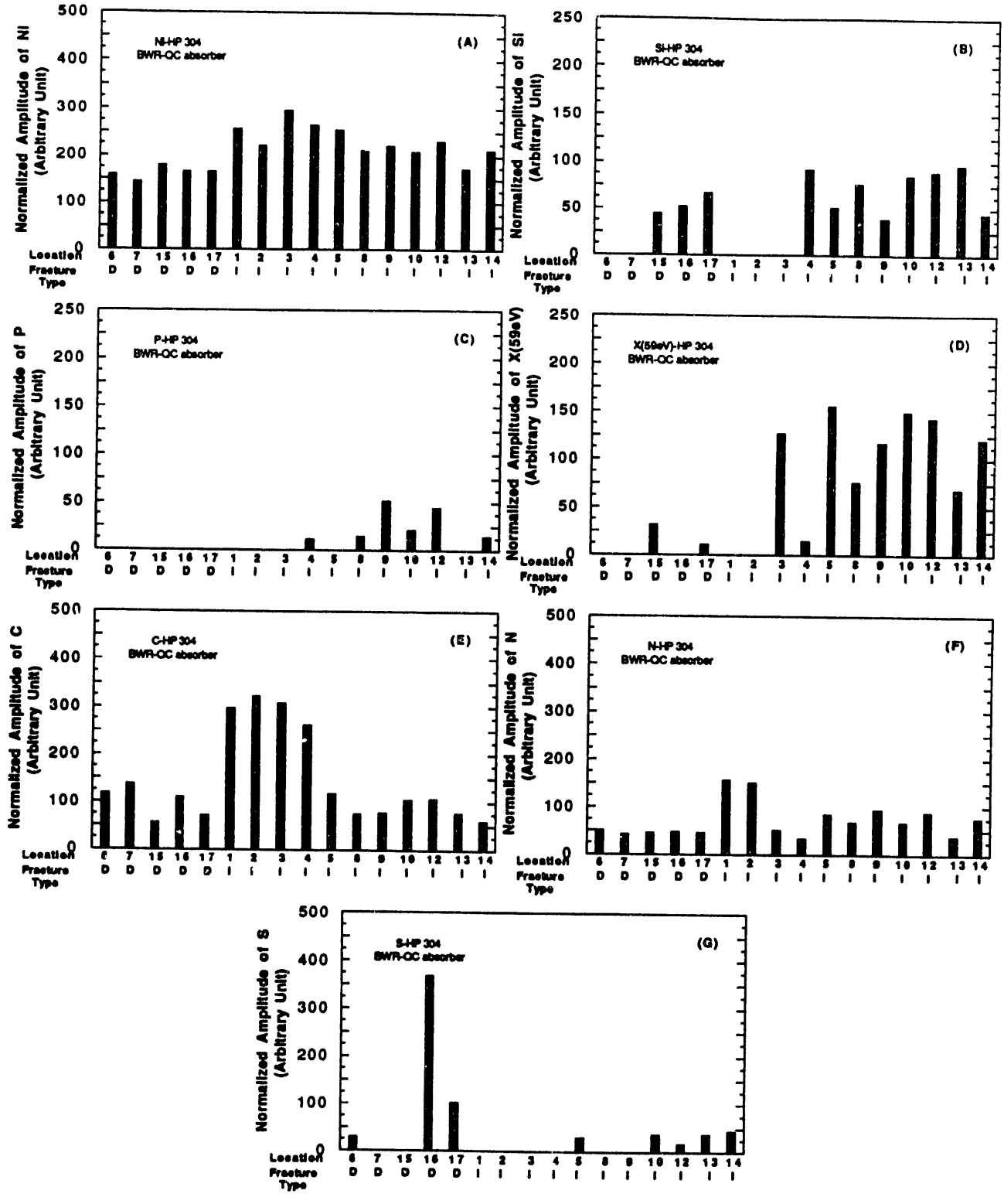

Fig 8. Normalized amplitudes of (a) Ni, (b) Si, (c) P, (d) an unidentified element (denoted $X_{59\text{-}eV}$), (e) C, (f) N, and (g) S that were obtained from ductile- (denoted by letter D) and intergranular- (I) fracture surfaces of HP Heat 304-CD absorber tube irradiated in BWR-QC to fluence of ≈2.0 x 10^{21} n cm^{-2} (E >1 MeV).

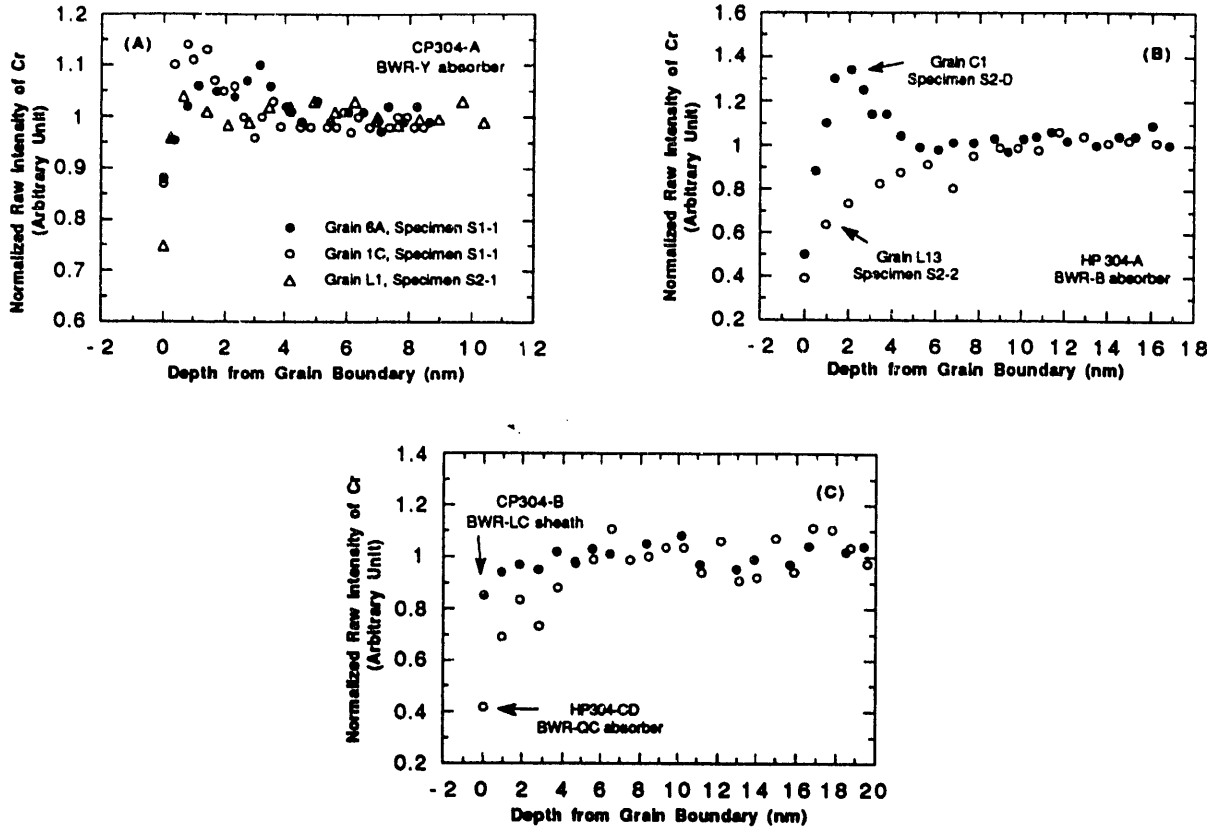

Fig 9. Grain boundary Cr-depletion profiles of (A) CP304-A absorber tube irradiated to ≈2.0 x 10^{21} n cm^{-2}, (B) HP304-A absorber tube, ≈1.4 x 10^{21} n cm^{-2}, and (C) HP304-CD absorber tube and CP304-B sheath, ≈2.0 x 10^{21} n cm^{-2}.

Table 3. Summary of Minimum Grain Boundary Cr Concentration of High- and Commercial-Purity Type 304 Stainless Steel BWR Components Determined by the AES Depth-Profile Technique.

Material and Heat	Component Code	Service Reactor	Fluence (E > 1 MeV), 10^{21} n·cm^{-2}	Minimum Cr Content, wt. %
HP304 -A	V-AT[a]	BWR-B	1.4	7.9-9.3
HP304-B	V-AT[a]	BWR-B	-	-
HP304-CD	V-AT[a]	BWR-B	-	-
HP304-CD	QC-AT[b]	BWR-QC	2.0	7.8
CP304 -A	BL-AT[c]	BWR-Y	2.0	12.8-14.8
CP304 -B	LC-S[d]	BWR-LC	2.0	15.9

[a]High-purity (HP) neutron absorber tubes, OD = 4.78 mm, wall thickness = 0.63 mm.
[b]High-purity neutron absorber tubes, OD = 4.78 mm, wall thickness = 0.63 mm.
[c]Commercial-purity neutron absorber tubes, OD = 4.78 mm, wall thickness = 0.79 mm
[d]Commercial-purity control blade sheath, thickness 1.22 mm.

Discussion

It is difficult to explain the significant IGSCC in the HP absorber tube specimens of Heat HP304-A or -CD on the basis of Si or P segregation, because segregation of the elements in the HP heats was negligible. Likewise, it is difficult to explain the negligible SCC susceptibility of the CP sheath specimens on the basis of a mechanism in which IASCC is controlled by Si or P segregation, because the segregation of impurities was significant in the sheath specimens. Therefore, it seems evident that grain-boundary segregation of Si or P is not the mechanism of IASCC, as has often been suspected. Lack of correlation between IGSCC susceptibility and Si[21] or P[18,19] segregation in Type 304 SS has also been reported by other investigators.

Percent IGSCC obtained from the present SSRT tests (Fig. 4) could be correlated well with minimum grain-boundary Cr levels (Table 3). This is shown in Fig. 10 where results for IGSCC of irradiated Type 304 SS are consistent with a mechanism in which irradiation-induced Cr depletion plays the primary role, at least in an environment similar to the present simulated BWR water.

The results presented are qualitatively similar to those reported by Bruemmer et al.,[17] who conducted SSRT tests on Type 304 SS specimens in which simulated Cr depletion was produced by iterative thermal sensitization and desensitization. In such specimens, the Cr depletion profile was significantly wider than in the present BWR components (i.e., ≈30 vs. ≈4 nm), and as a result, measurement of minimum Cr content with a Vacuum Generator Model HB501 field-emission-gun scanning transmission electron microscope (FEG-STEM) was relatively facilitated. Similar measurements of minimum Cr concentration with the HB501 STEM have also been reported by Norris et al. for 20Cr-25Ni-Nb SS that was irradiated at ≥354°C. From their analysis, the Cr depletion width of fuel cladding of an advanced gas-cooled reactor was at least ≈20 nm or larger. For these relatively wider Cr-depleted zones, minimum grain-boundary Cr contents of ≈10 wt.% were measured by the EDS technique in the HB501 STEM, which has a nominal probe size of ≈2.5 nm. The minimum Cr level of ≈10 wt.% measured by Bruemmer et al.[17] for a specimen irradiated by ions at 500°C to ≈5 dpa was found to be in good agreement with the theoretically predicted value of ≈8-9 wt.%. For irradiation by neutrons to ≈1-2 dpa at 289°C, minimum Cr concentration is predicted to be similar but depletion width is predicted to be much narrower.[17] Thus, a minimum Cr concentration of ≈8-9 wt.% is expected for the present BWR components that were irradiated to a fluence of ≈2 x 10^{21} n cm^{-2}.

For extremely narrow Cr depletion profiles, such as those in Fig. 9, it would be difficult to determine a true grain-boundary minimum Cr content by the EDS technique in a STEM such as the HB501 STEM. Results in Fig. 9 indicate that, to determine the true minimum Cr level in a BWR-irradiated component, at least three to four data points must be obtained at 0-1 nm away from a grain boundary and that measurements must be sensitive enough to the difference in true Cr content over a narrow interval (e.g., 0.3-0.5 nm). Both features may be too difficult to achieve in the EDS mode in the HB501 STEM because of the limited resolution, i.e. a resolution that may be sufficient to measure a wider depletion profile but insufficient to measure the minimum Cr within ≈1 nm in BWR-irradiated components.

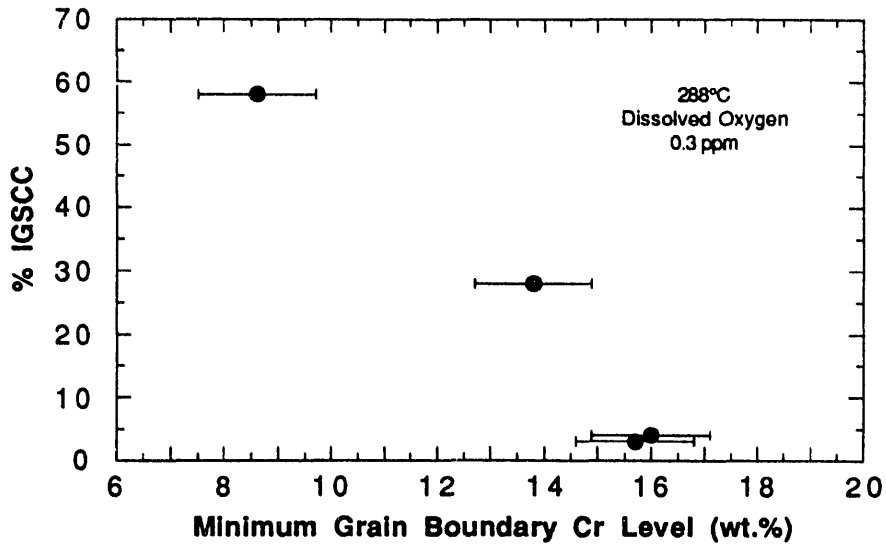

Fig. 10. Percent IGSCC vs. minimum grain boundary Cr content determined from SSRT tests and AES analysis of HP and CP Type 304 SS BWR components.

A typical image of a grain boundary itself is as wide as ≈1-2 nm in bright-field, and an angle between the incident beam and a grain boundary as small as 1° will produce an ≈1-nm shift in grain-boundary positions on the top and bottom planes in an ≈60-nm-thick foil. The data reported in Refs. 8, 9, 20, and 21 were obtained from EDS signals measured in HB501 STEM at 1-nm intervals, a distance significantly smaller than the nominal probe size of ≈2.5 nm. In these studies, no minimum Cr level lower than 15 wt.% was reported for BWR-irradiated specimens.

It is well known that a minimum Cr level measured by the STEM-EDS technique to is sensitive to a number of factors, such as effective probe size, beam broadening, local foil thickness variation, presence of ultrafine irradiation-induced precipitates or clusters, composition inhomogeneity produced near radiation-induced defects and "black-dot" loops, grain boundary contamination from foil thinning, formation of chromium-oxide surface film, spurious fluoresce Cr X-ray produced because of the radioactive decay of isotopes, and angle between the incident beam and grain boundary. The case for using the HB501 STEM has been treated elegantly by Titchmarsh and Vatter.[23] The minimum Cr concentration measured with EDS is strongly affected by beam broadening, probe size, and local foil thickness, although the width of the Cr depletion profile is relatively less sensitive to these factors.

Because of the above limitations, it would be difficult to determine the true minimum Cr concentration on grain boundaries of BWR-irradiated specimens from EDS data such as those reported in Refs. 8, 9, 20, and 21, and true grain-boundary Cr concentration will always be lower than measured values. Accordingly, it is believed that a mechanism based on grain-boundary Cr concentration cannot be discounted for BWR-irradiated components based on EDS measurements of Cr-depletion profiles by presently available FEG-STEM. A

next-generation improved FEG-STEM may be able to provide improved data from analysis by EDS or electron energy loss spectroscopy (EELS) with smaller probes and greatly reduced excitation volume. In contrast to EDS in which excitation of bulky volume is involved, measurement by the AES depth-profiling technique is sensitive to concentrations of surface layers only. Thus, the measured Cr contents given in Table 3 are believed to be close to actual values, and grain-boundary Cr concentration is believed to be a primary factor that controls IGSCC susceptibility of BWR-irradiated Type 304 austenitic stainless steels According to Fig. 10, IGSCC susceptibility in water at ≈288°C is expected to be negligible when minimum grain-boundary Cr concentration exceeds ≈15 wt.%.

HP-grade specimens that exhibited relatively higher susceptibilities than CP-grade specimens either contained high N (HP304-A) or showed N segregation (HP304-CD). It is not clear if this observation indicates a deleterious effect of N, at least in HP Type 304 SS. It can be only stated that, at this time, we cannot exclude a mechanism that is based on a synergism between segregation and transmutation of N (to H), or even segregation and transmutation of B. Evidence of boron segregation was not observed in all examined specimens, probabably because of transmutation to He and Li. Lithium exhibits AES peaks at ≈43 and ≈58 eV. The former peak will be superimposed on the $Fe_{47\text{-}eV}$ peak. Therefore, at this time, we can neither discount nor prove that the unidentified peak $X_{59\text{-}eV}$ indeed originated from Li, and hence, from segregated B. Li on grain boundaries will react with hydrogen to form lithium hydride, which is expected to cause grain boundary decohesion. If a transmutation-related synergism controls IASCC, effects of incident neutron flux, rates of transmutation, strain rate, and intragranular trapping of H, He, and Li will be important because these factors will influence grain boundary concentration of hydrogen or helium. It is also likely that results of laboratory CERT tests and in-reactor performance are significantly different because of the differences in incident neutron flux and strain rate. Also, we cannot exclude a possibility that grain boundary Cr concentration is the primary factor during laboratory CERT tests; however, a transmutation-related synergism is the primary process for certain components during reactor operation.

Behavior of Type 304 SS and Types 348 and 316 SS may be quite different because of the likelihood that the oversized Nb and Mo atoms in the two latter heats strongly influence defect recombination, vacancy trapping, vacancy distribution, and hence, Cr depletion. Thus, it may be relatively easier to prevent significant Cr depletion in Type 348 or 316 than in Type 304 SS. In such a situation, N and B segregation and transmutation may be the only operative process remaining (to promote IASCC), and an HP low-N heat may effectively suppress IASCC. However, this may not be the case in Type 304 SS. An HP heat of Type 304 SS may exhibit a relatively more pronounced Cr depletion than a CP heat because the vacancy-trapping role of Nb, Mo, or impurities is either absent or negligible.

Conclusions

1. SSRT tests were conducted on specimens of several heats of commercial- and high-purity (CP and HP) grades of Type 304 SS obtained from BWR neutron absorber tubes and a control blade sheath in simulated BWR water. Thre susceptibility of the CP-grade sheath to IGSCC was significantly lower than that of neutron absorber tubes fabricated from another CP-grade heat. Susceptibilities of two HP-grade heats

were significantly higher than those of the CP absorber tubes and sheath or CP-grade BWR dry tubes reported in the literature.

2. Grain-boundary segregation and depletion in the CP sheath and CP neutron absorber tube was comparable, except for the indication of C segregation and grain boundary Cr concentration. Grain-boundary segregation of impurities in the HP absorber tubes were negligible, except for segregation of N and the unidentified element that gives rise to 59-eV in Auger spectra in one of the HP heats.

3. IGSCC susceptibilities of the CP and HP BWR components could not be correlated with grain-boundary segregation of Si or P, indicating that neither Si nor P segregation is an important process in IASCC.

4. The relative susceptibilities of the HP and CP neutron absorber tubes and control blade sheath to IGSCC could be correlated well with grain-boundary Cr concentration, indicating that grain-boundary depletion of Cr is a major process in IASCC.

5. A mechanism based on a synergism that involves grain-boundary segregation and transmutation of N (to H) and segregation and transmutation of B (to He and Li) cannot be excluded. If such a synergism controls IASCC, effects of incident neutron flux and relative rates of transmutation and straining would be important factors; hence, results of laboratory CERT tests and in-reactor performance could be significantly different. Relative importance of Cr-depletion and transmutation-related synergistic processes may be different during laboratory CERT test and in-reactor operation for certain components.

Acknowledgments

D. A. Donahue and G. J. Talaber contributed to the experimental effort in this program. A. G. Hins and A. Purohit conducted SEM analysis of the fractured specimens. The BWR components were obtained through the kind assistance of Drs. R. Kohli and A. J. Jacobs. This work was sponsored by the Office of Nuclear Regulatory Research, U.S. Nuclear Regulatory Commission. The authors are grateful to Drs. J. Muscara and W. J. Shack for helpful discussions.

References

1. W. L. Clark and A. J. Jacobs, *Effect of Radiation Environment on SCC of Austenitic Materials*, in Proc. 1st Int. Symp. Environmental Degradation of Materials in Nuclear Power Systems - Water Reactors, National Association of Corrosion Engineers, Houston, pp. 451-461 (1984).

2. F. Garzarolli, D. Alter, P. Dewes, and J. L. Nelson, *Deformability of Austenitic Stainless Steels and Ni-Base Alloys in the Core of a Boiling and Pressurized Water Reactor*, in Proc. 3rd Int. Symp. Environmental Degradation of Materials in Nuclear Power Systems

- Water Reactors, G. J. Theus and J. R. Weeks, eds., The Metallurgical Society, Warrendale, PA, pp. 657–664 (1988).

3. H. Hanninen and I. Aho-Mantila, *Environment-Sensitive Cracking of Reactor Internals*, ibid., pp. 77–92.

4. K. Fukuya, S. Nakahigashi, S. Ozaki, M. Teresawa, and S. Shima, *Grain Boundary Segregation of Impurity Atoms In Irradiated Austenitic Stainless Steels*, ibid., pp. 665–671.

5. A. J. Jacobs, G. P. Wozaldo, K. Nakata, T. Yoshida, and I. Masaoka, *Radiation Effects on the Stress Corrosion and Other Selected Properties of Type-304 and Type-316 Stainless Steels*, ibid., pp. 673–681.

6. E. P. Simonen and R. H. Jones, *Calculated Solute Segregation Kinetics Related to Irradiation-Assisted Stress Corrosion Cracking*, ibid., pp. 683–690.

7. A. J. Jacobs, R. E. Clausing, L. Heatherly, and R. M. Kruger, *Irradiation-Assisted Stress Corrosion Cracking and Grain Boundary Segregation in Heat-Treated Type 304 SS*, in Effects of Radiation on Materials: 14th Int. Symp., Vol. I, ASTM STP 1046, N. H. Packan, R. E. Stoller, and A. S. Kumar, eds., American Society for Testing and Materials, Philadelphia, pp. 424–436 (1989).

8. A. J. Jacobs, R. E. Clausing, M. K. Miller, and C. Shepherd, *Influence of Grain Boundary Composition on the IASCC Susceptibility of Type 348 Stainless Steel*, in Proc. 4th Int. Symp. Environmental Degradation of Materials in Nuclear Power Systems – Water Reactors, National Association of Corrosion Engineers, Houston, pp. 14–21 to 14–45 (1990).

9. C. M. Shepherd and T. M. Williams, *Simulation of Microstructural Aspects of IASCC in Water Reactor Core Components*, ibid., pp. 14–11 to 14–20.

10. P. L. Andresen, F. P. Ford, S. M. Murphy, and J. M. Perks, *State of Knowledge of Radiation Effects on Environmental Cracking in Light Water Reactor Core Materials*, ibid., pp. 1–83 to 1–121.

11. H. M. Chung and W. E. Ruther, in *Environmentally Assisted Cracking in Light Water Reactors: Semiannual Report, April-September 1990*, NUREG/CR–4667 Vol. 11, ANL–91/9, pp. 16–22 (April 1991).

12. H. M. Chung and W. E. Ruther, in *Environmentally Assisted Cracking in Light Water Reactors: Semiannual Report, October 1990-March 1991*, NUREG/CR–4667 Vol. 12, ANL–91/24, pp. 37–54 (August 1991).

13. H. M. Chung, W. E. Ruther, and A. G. Hins, in *Environmentally Assisted Cracking in Light Water Reactors: Semiannual Report, April-September 1991*, NUREG/CR–4667 Vol. 13, ANL–92/6, pp. 20–36 (March 1992).

14. A. J. Jacobs, General Electric Co., San Jose, CA, private communications.

15. M. Kodama, S. Nishimura, J. Morisawa, S. Shima, S. Suzuki, and M. Yamamoto, *Effects of Fluence and Dissolved Oxygen on IASCC in Austenitic Stainless Steels*, Proc. 5th Int. Symp. Environmental Degradation of Materials in Nuclear Power Systems – Water Reactors, American Nuclear Society, La Grange Park, IL, pp. 948-954 (1992).

16. H. M. Chung, W. E. Ruther, J. E. Sanecki, and T. F. Kassner, *Irradiation-Induced Sensitization and Stress Corrosion Cracking of Type 304 Stainless Steel Core-Internal Components*, ibid., pp. 795-805.

17. S. M. Bruemmer, L. A. Charlot, and E. P. Simpson, *Irradiation-Induced Chromium Depletion and Its Influence on Intergranular Stress Corrosion Cracking of Stainless Steels*, ibid., pp. 821-826.

18. J. M. Cookson, R. D. Carter, D. L. Damcott, M. Atzmon, G. S. Was, and P. L. Andresen, *Stress Corrosion Cracking of High-Energy Proton-Irradiated Stainless Steels*, ibid., pp. 806-813.

19. K. Fukuya, K. Nakata, and A. Horie, *An IASCC Study Using High Energy Ion Irradiation*, ibid., pp. 814-820.

20. K. Asano, K. Fukuya, K. Nakata, and K. Kodama, *Changes in Grain Boundary Composition by Neutron Irradiation on Austenitic Stainless Steels*, ibid. pp. 838-843.

21. A. J. Jacobs, C. M. Shepherd, G. E. C. Bell, and G. P. Wozaldo, *High-Temperature Solution Annealing as an IASCC Mitigation Technique*, ibid., pp. 917-934.

22. D. I. R. Norris, C. Baker, and J. M. Titchmarsh, *Compositional Profiles at Grain Boundaries in 20%Cr/25%Ni/Nb Stainless Steel*, Proc. Symp. on Radiation-Induced Sensitization of Stainless Steels, D. I. R. Norris ed., Central Electricity Generating Board, Berkeley, England, pp. 86-98 (1987).

23. J. M. Titchmarsh and I. A. Vatter, *Measurement of Radiation-Induced Segregation Profiles by High Spatial Resolution Electron Microscopy*, ibid., pp. 74-85.

END

DATE FILMED

1/27/93